GEOLOGY | THE GEOLOGICAL SOCIETY OF AMERICA®

https://doi.org/10.1130/G49649.1

Manuscript received 6 April 2021
Revised manuscript received 1 September 2021
Manuscript accepted 16 November 2021

Published online 3 February 2022

Quantifying volcanism and organic carbon burial across Oceanic Anoxic Event 2

Nina M. Papadomanolaki[1]*, Niels A.G.M. van Helmond[1], Heiko Pälike[2], Appy Sluijs[1] and Caroline P. Slomp[1]
[1]Department of Earth Sciences, Utrecht University, 3584 CB Utrecht, Netherlands
[2]MARUM–Center for Marine Environmental Sciences, University of Bremen, 28359 Bremen, Germany

ABSTRACT

Oceanic Anoxic Event 2 (ca. 94 Ma; OAE2) was one of the largest Mesozoic carbon cycle perturbations, but associated carbon emissions, primarily from the Caribbean large igneous province (LIP) and marine burial fluxes, are poorly constrained. Here, we use the carbon cycle box model LOSCAR-P to quantify the role of LIP volcanism and enhanced marine organic carbon (C_{org}) burial as constrained by the magnitude and shape of the positive stable carbon isotope ($\delta^{13}C$) excursion (CIE) in the exogenic carbon pool and atmospheric pCO_2 reconstructions. In our best fit scenario, two pulses of volcanic carbon input—0.065 Pg C yr^{-1} over 170 k.y. and 0.075 Pg C yr^{-1} over 40 k.y., separated by an 80 k.y. interval with an input of 0.02 Pg C yr^{-1}—are required to simulate observed changes in $\delta^{13}C$ and pCO_2. Reduced LIP activity and C_{org} burial lead to pronounced pCO_2 reductions at the termination of both volcanic pulses, consistent with widespread evidence for cooling and a temporal negative trend in the global exogenic $\delta^{13}C$ record. Finally, we show that observed leads and lags between such features in the records and simulations are explained by differences in the response time of components of the carbon cycle to volcanic forcing.

INTRODUCTION

Oceanic Anoxic Event 2 (OAE2) was an ~430–930-k.y.-long (Voigt et al., 2008; Gangl et al., 2019) interval of high atmospheric pCO_2 and temperatures that is generally attributed to greenhouse gas emissions from large igneous province (LIP) magmatism, primarily the Caribbean–Colombian LIP (CLIP) (Turgeon and Creaser, 2008; Jenkyns, 2010). The greenhouse cycle promoted deoxygenation and enhanced burial of organic carbon (C_{org}) (e.g., Kuypers et al., 2002). A positive carbon isotope ($\delta^{13}C$) excursion (CIE), consisting of a stepped increase of 3‰ (average; Owens et al., 2018) to a maximum "a," a negative excursion ("trough"; termed the Plenus CIE; O'Connor et al., 2020), a second maximum "b," a plateau, and a gradual return to pre-OAE2 values (Fig. 1), marks OAE2 in sedimentary records (e.g., Jenkyns, 2010). Records of pCO_2 generally show an increase across the onset of OAE2, two phases of lower values associated with the carbon isotope maxima, and another increase within the Plenus CIE (e.g., Sinninghe Damsté et al., 2008; Barclay et al., 2010; Kuhnt et al., 2017). Presumably, both of these drops in pCO_2 are associated with cooling phases, one of which is the stratigraphically complex Plenus Cold Event (see the Supplemental Material[1]; O'Connor et al., 2020).

Trends and the timing of key features in $\delta^{13}C$ and pCO_2 records across OAE2 are determined by LIP volcanism and enhanced C_{org} burial. LIP emission rates are estimated at between 0.03 and 4.7 Pg C yr^{-1} and total emission masses between 14,000 and 46,000 Pg C (Table S1 in the Supplemental Material). C_{org} burial records (e.g., Kolonic et al., 2005) suggest burial of a total of at least 41,000 Pg C across OAE2 (Owens et al., 2018). The ~25% drop in pCO_2 marking $\delta^{13}C$ maximum "a" has been attributed to increased C_{org} burial (e.g., Barclay et al., 2010) and/or decreased LIP volcanism (e.g., Clarkson et al., 2018). The Plenus CIE may be the result of decreased C_{org} burial following the reduction in pCO_2 and/or an increase in LIP volcanism. Yet, a comprehensive, mechanistically plausible scenario for volcanic input and excess C_{org} burial that explains all observations is still lacking.

In this study, we present the first scenario for LIP volcanism and C_{org} burial for OAE2 that reproduces the shape and magnitude of the CIE and the timing of its major features relative to pCO_2 reconstructions (Fig. 1). We use the carbon cycle box model LOSCAR-P (Komar and Zeebe, 2017) to assess the impact of a range of volcanic emission scenarios on sedimentary $\delta^{13}C$ records, pCO_2, and C_{org} burial.

CARBON CYCLE MODEL SETUP AND CONSTRAINTS

The LOSCAR-P model with the Paleocene–Eocene model configuration represents the open ocean, including the Tethys Ocean, but not marginal and restricted environments (Zeebe, 2012; Komar and Zeebe, 2017). It enables us to study bulk carbonate $\delta^{13}C$ and atmospheric pCO_2 as a function of volcanism, weathering, and marine C_{org} burial. The redox-dependency of C_{org} and phosphorus burial enhances phosphorus recycling relative to C_{org} upon ocean deoxygenation (Komar and Zeebe, 2017). We used the setup of Komar and Zeebe (2017) but with increased initial calcium (25 mmol kg^{-1}) and magnesium (35 mmol kg^{-1}) concentrations (Zeebe and Tyrrell, 2019) and a mid-Cretaceous $\delta^{13}C_{org}$ value (−28‰; Kump and Arthur, 1999).

The onset of volcanism likely preceded the OAE2 onset by <60 k.y. (Jones et al., 2020). A 1–3‰ negative CIE precedes the positive CIE in some $\delta^{13}C_{org}$ records (Kuroda et al., 2007; Kalanat et al., 2018). The OAE2 CIE ranges in magnitude from 1‰ to 7‰ (average 3‰; Owens et al., 2018), and the Plenus CIE drop ranges from 0.5% to 4‰ (Forster et al., 2007; Voigt et al., 2007). Atmospheric pCO_2 increased by ~20% over background values at the onset of OAE2 (~460 ± 100 ppm; Barclay et al., 2010)

*Current address: Aix-Marseille Universite, CNRS, IRD, INRA, Coll. France, CEREGE, Aix-en-Provence, France; E-mail: n.papadomanolaki@uu.nl

[1]Supplemental Material. Supplemental information and methods, Figures S1–S4, and Tables S1 and S2. Please visit https://doi.org/10.1130/GEOL.S.18173069 to access the supplemental material, and contact editing@geosociety.org with any questions.

CITATION: Papadomanolaki, N.M., et al., 2022, Quantifying volcanism and organic carbon burial across Oceanic Anoxic Event 2: Geology, v. 50, p. 511–515, https://doi.org/10.1130/G49649.1

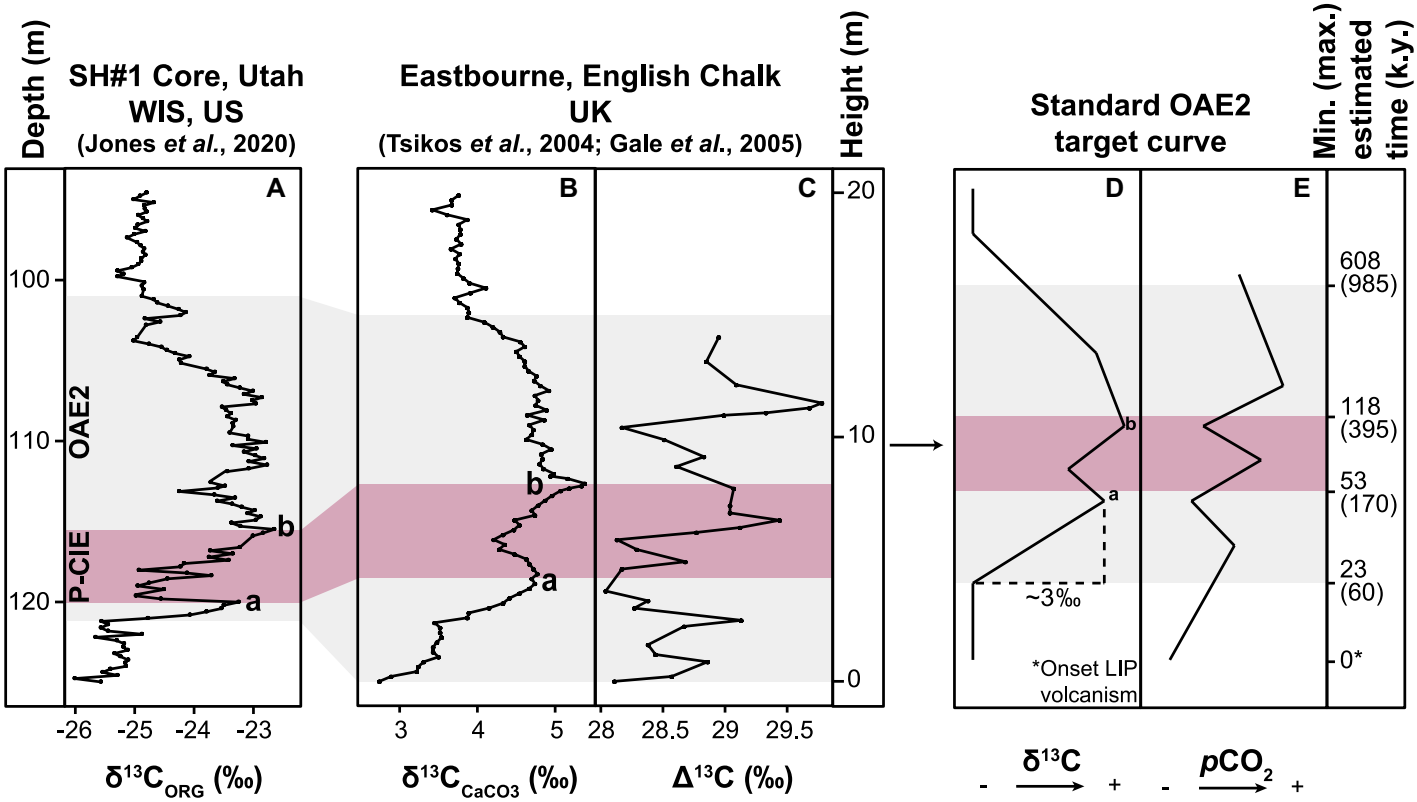

Figure 1. Stable carbon isotope records across Oceanic Anoxic Event 2 (OAE2) for the Western Interior Seaway (WIS, western United States). (A) Organic $\delta^{13}C$ for the SH#1 Core (Utah, USA), Jones et al. (2020); and (B) carbonate $\delta^{13}C$ for the English Chalk (Eastbourne, UK), Tsikos et al. (2004). P-CIE—Plenus carbon isotope excursion. The two distinct $\delta^{13}C$ maxima are labeled "a" and "b". The difference between $\delta^{13}C_{org}$ and $\delta^{13}C_{carb}$ for (C) Eastbourne is shown as a proxy for pCO_2 (Gale et al., 2005). (D,E) Target curves for our simulations as idealized records of (D) the positive carbon isotope ($\delta^{13}C$) excursion (CIE), with an initial 3‰ increase (Owens et al., 2018), and (E) pCO_2. Target curves are based on the data compilation of O'Connor et al. (2020). Gray band represents OAE2. Purple band shows the Plenus $\delta^{13}C$ trough. Minimum (maximum) ages are relative to the onset of the main pulse of enhanced volcanism (0 k.y.; see the Supplemental Material [see footnote 1] for age derivations). LIP—large igneous province.

and decreased by ~25% before the Plenus CIE (e.g., Sinninghe Damsté et al., 2008; Barclay et al., 2010; Jarvis et al., 2011). We evaluated our emission scenarios with these constraints to simulate the key characteristics of the OAE2 carbon cycle.

We increased the model volcanic CO_2 flux ($\delta^{13}C_{volc}$: −5‰) to force our simulations. The impact of redox-dependent C_{org} and P burial on $\delta^{13}C$ was tested with a maximum excess input rate of 0.2 Pg C yr^{-1} over 90 k.y., with and without redox-dependency. The effect of emission rate and duration was tested in four simulations of 90 k.y. and 540 k.y., with maximum emission rates of 0.2 Pg C yr^{-1} and 0.04 Pg C yr^{-1}, and redox-dependent burial. All scenarios started with a linear rate increase over 20 k.y., which reproduced the ~60 k.y. lag, and ended with a 20 k.y. linear recovery to zero. Then we conducted sensitivity analyses for the rate, mass, duration, and shape of volcanism scenarios (Fig. S1) and derived a best-fit scenario. Information about further sensitivity analyses with thermogenic methane ($\delta^{13}C_{CH4}$: −35‰) and reduced circulation are provided in the Supplemental Material. Due to the various processes affecting $\delta^{13}C$ signatures, the results of $\delta^{13}C$ models are non-unique. We minimized the impact on our results by constraining them with atmospheric pCO_2 and C_{org} burial rates in addition to $\delta^{13}C$ variations.

RESULTS

All scenarios forced by volcanism result in a small negative CIE (Fig. 2), followed by a larger positive CIE that is mainly caused by enhanced, redox-dependent C_{org} burial (Figs. 2A, 2B, and 2D). In all cases (Fig. 2E), the peak in $\delta^{13}C$ is preceded by a peak in pCO_2. Following the return to background volcanic activity, $\delta^{13}C$ and pCO_2 recover to their background values on time scales of 400 k.y. and 100 k.y., respectively.

The maximum value of the positive CIE and pCO_2 rise varies with the duration and rate of volcanic input (Figs. 2C–2E). From the 90 k.y. scenario to the 540 k.y. scenario, the pCO_2 peak shifts from the end of the negative CIE interval to the increasing $\delta^{13}C$ section of the positive CIE. In the 90 k.y. scenarios, the recovery of pCO_2 and $\delta^{13}C$ to background values begins immediately after their maximum. For the 540 k.y. scenarios, the final recovery is preceded by a $\delta^{13}C$ decrease and a second peak. In these simulations, the minimum in pCO_2 coincides with the first $\delta^{13}C$ maximum and occurs within the interval of enhanced volcanic activity, while volcanism decreases within the $\delta^{13}C$ trough. This is not the case for the 90 k.y. scenarios.

TWO VOLCANIC PULSES

In our simulations, a negative $\delta^{13}C$ excursion precedes the positive CIE, which is not a common feature (e.g., Tsikos et al., 2004), but it is present in several OAE2 $\delta^{13}C_{org}$ records (e.g., Kuroda et al., 2007). This negative $\delta^{13}C$ excursion may have been enhanced or masked by site-specific processes. The simulations show that it could be forced by volcanic CO_2 emissions alone.

Two $\delta^{13}C$ maxima, a negative CIE between them, and a decrease in pCO_2 near the first maximum are reproduced only by the longer (540 k.y.) forcing scenarios and are most distinct in the high emission scenario (0.2 Pg C yr^{-1}). Yet, the large positive CIE (~7.9‰), high maximum pCO_2 (~4000 ppmv), and large drop in pCO_2 (45%) for this scenario far exceed OAE2 variability estimates, while there is no clear increase in pCO_2 within the negative CIE (Fig. 1). A variable emissions scenario is therefore required to

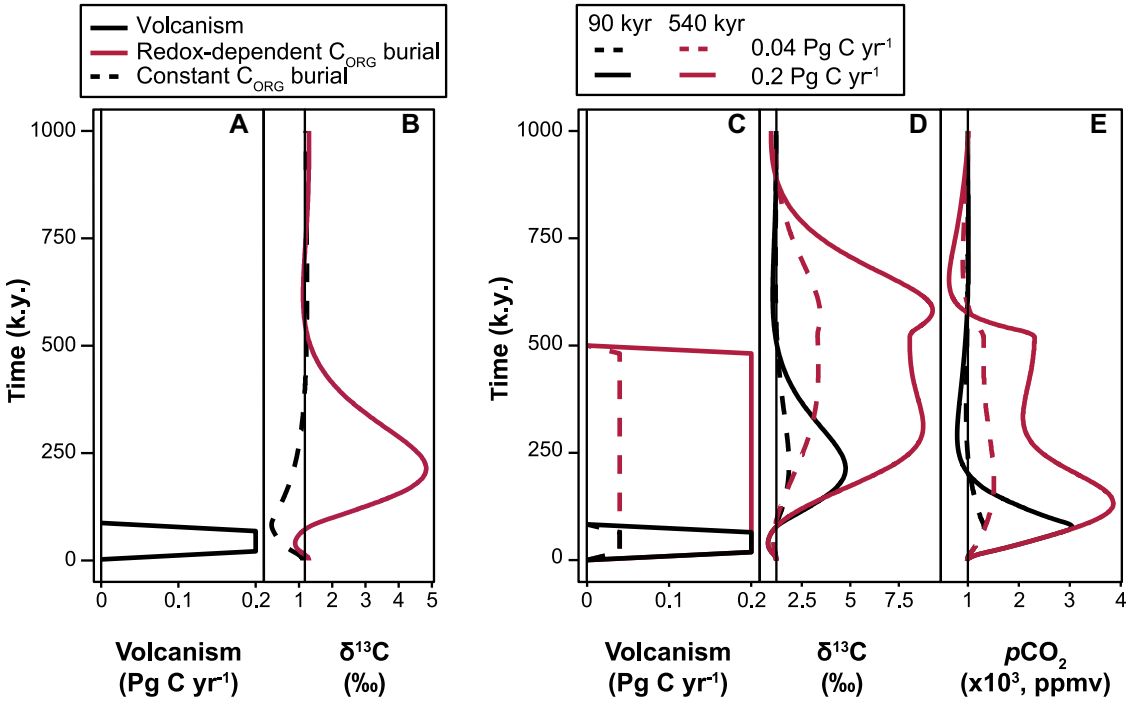

Figure 2. Response of $\delta^{13}C$ and pCO_2 to increased volcanism. The effect of excess volcanic emissions (black solid line) on (A) 14,000 Pg C (90 k.y.); and (B) $\delta^{13}C$, with constant (black dashed line) and redox-dependent C_{org} and phosphorus burial (red line). (C) The effect of additional volcanism scenarios, with maximum rates of 0.04 Pg C yr^{-1} (dashed lines) and 0.2 Pg C yr^{-1} (solid lines) over 90 k.y. (black) and 540 k.y. (red), on (D) $\delta^{13}C$ and (E) pCO_2, with redox-dependent burial. Vertical lines indicate the steady-state value in each panel.

reproduce the key features of the $\delta^{13}C_{bulk}$ and pCO_2 records.

In our best-fit scenario, LIP volcanism consists of two pulses, 0.065 Pg C yr^{-1} over 170 k.y. and 0.075 Pg C yr^{-1} over 40 k.y., separated by an 80 k.y. interval of 0.02 Pg C yr^{-1} (Fig. 3A; see the Supplemental Material). The duration of the first pulse and the decrease from the first maximum both last 20 k.y. The increase, as well as the termination, of the second pulse last 80 k.y. The total duration of LIP activity is 490 k.y. with a total emission mass of ~24,000 Pg C (Table S1). Multiple volcanic pulses are supported by osmium isotope records (Sullivan et al., 2020). Additionally, Clarkson et al. (2018) reproduce their uranium isotope records using a two-pulse CO_2 model emission scenario. Our two-pulse scenario reproduces the main characteristics of our target scenario ("a", Plenus CIE, "b") and the relative timing between $\delta^{13}C$ and pCO_2 (Figs. 1 and 3). The initial $\delta^{13}C$ increase to "a" (2.96‰) is equal to the global average of 3‰ (Owens et al., 2018), and our simulated Plenus CIE (0.52‰) has a magnitude similar to the drop in $\delta^{13}C_{carb}$ at Eastbourne (Tsikos et al., 2004) and in $\delta^{13}C_{org}$ at Ocean Drilling Program site 1276 (Sinninghe Damsté et al., 2010). Also, the simulated 35% (660 ppmv) drop in atmospheric pCO_2 agrees with proxy reconstructions (Sinninghe Damsté et al., 2008; Barclay et al., 2010; Jarvis et al., 2011).

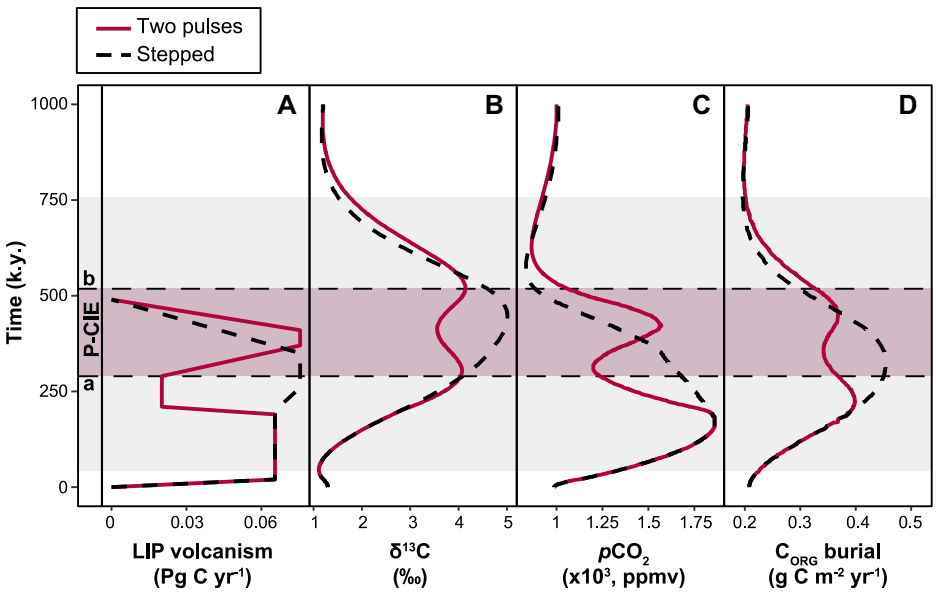

Figure 3. Key model output for Oceanic Anoxic Event 2 (OAE2) simulations. (A) Large igneous province (LIP) volcanic forcing (Pg C yr^{-1}). (B) Bulk $\delta^{13}C$ (‰). (C) atmospheric pCO_2 (ppm). (D) C_{org} burial rates (g C m^{-2} yr^{-1}). Two forcing scenarios are used: two pulses separated by a reduction (solid red line) and a stepped increase (black dashed line). Horizontal dashed lines indicate the positions of the two $\delta^{13}C$ maxima "a" and "b". Gray area represents OAE2. Purple bar shows the Plenus carbon isotope excursion.

Our simulated OAE2, from onset to "b," has an overall duration of ~500 k.y. Assuming that the plateau and recovery phases lasted several hundreds of thousands of years. (Gangl et al., 2019), our duration is in line with longer estimates (³700 k.y.; Jones et al., 2020). The onset of our CIE up to "a" is considerably longer (250 k.y.) than the longest estimate (110 k.y.; Li et al., 2017). This may be due to the lack of proto-North Atlantic restriction and/or the underrepresentation of shallow and restricted environments (e.g., epicontinental seas; see the Supplemental Material) where additional C_{org} could be buried. For the same CO_2 emission scenario, more C_{org} could potentially be buried in a simulation with Cenomanian–Turonian (C/T) paleogeography, which could result in a larger, and potentially more rapid, positive CIE. The duration of the Plenus CIE (200 k.y.) agrees with the estimate from the Western Interior Seaway (Jones et al., 2020) and further corroborates our two-pulse volcanism scenario.

VOLCANISM AND ITS EFFECT ON ORGANIC CARBON BURIAL

Our best fit scenario requires a total emission of ~24,000 Pg C by LIP volcanism, or more

if thermogenic methane production is included (Supplemental Material). With a magmatic CO_2 content of 0.5 wt% (0.2–0.6 wt%; Jones et al., 2016), or an emission of 0.0035 Pg C km^3 (Self et al., 2005), our scenario requires a LIP volume of 6.8×10^6 km^3. The CLIP has an estimated volume of 4×10^6 km^3 (Kerr, 1998), though a total of 20×10^6 km^3 of basalts erupted around the C/T boundary and OAE2 during the emplacement of the CLIP, the Madagascar LIP, and part of the Ontong–Java Plateau (Bond and Wignall, 2014).

The 500 k.y. duration of our scenario is short for LIP emplacement. Age constraints indicate that LIP magmatism generally spanned millions of years and often consisted of multiple phases (e.g., Bond and Wignall, 2014). A maximum of 4×10^6 km^3 of magma was erupted within <2 m.y. from the Late Permian Siberian Traps (Russia), causing a mass extinction (Reichow et al., 2009). Assuming the emplacement of 20×10^6 km^3 of within ~4 m.y. (Bond and Wignall, 2014), the average rate of eruption at the C/T boundary would be 2.5 times faster than at the Siberian Traps. Our best-fit, average emission rate is seven times larger than is estimated for the Siberian Traps, which seems high. The current resolution and precision of flood basalt dating does not allow us to directly evaluate our scenario, but osmium isotope records indicate that a 500 k.y. pulse of enhanced volcanism coincided with OAE2 (e.g., Du Vivier et al., 2015). Additionally, Joo et al. (2020) required the full mass of the CLIP emitted over 500 k.y. to simulate only the initial positive CIE of OAE2. The specifics of our emission scenarios may be further affected by pulse duration, basin morphology, and burial redox-sensitivity (see the Supplemental Material and Fig. S1); however, the general aspects of our best-fit scenario are plausible within the current constraints on Late Cretaceous LIP activity and the $\delta^{13}C$ and pCO_2 records.

We simulate two distinct maxima in C_{org} accumulation rates (Fig. 3D), which roughly double from ~0.2 to ~0.4 g C m^{-2} yr^{-1}, similar to the average increase at Tarfaya (Kolonic et al., 2005). Our increase exceeds that of Clarkson et al. (2018) (1.3 times pre-OAE2), but their resulting CIE (1.5‰) is only half the global average value. Maximum C_{org} burial (~0.125 Pg C yr^{-1}) is lower than those modeled by Nederbragt et al. (2004) and Owens et al. (2018) (~0.185 Pg C yr^{-1}), but our rates, expressed per unit surface area, and the relative change in burial are in general agreement with their work. The amount of excess C_{org} burial required for the 3‰ CIE in LOSCAR is ~9100 Pg C, which is roughly equal to the value required in the simulation by Owens et al. (2018) for an equivalent CIE. Our total simulated C_{org} burial from the onset of OAE2 until "b" is ~51,400 Pg C (excess burial: ~20,500 Pg C), consistent with previous calculations (41,000–70,000 Pg C; Owens et al., 2018).

The relative impact of changes in volcanism and enhanced C_{org} burial on the carbon cycle during OAE2 are still heavily debated (O'Connor et al., 2020). In our LIP volcanism scenario, we show that two pulses separated by a reduction are critical for reproducing the Plenus CIE, a large decrease in pCO_2 that is consistent with temperature records, as well as the second peaks in $\delta^{13}C$ and pCO_2, without exceeding the average 3‰ OAE2 CIE (Figs. 2 and 3). The pCO_2 drop is forced by decreased volcanism and increased C_{org} burial and silicate weathering (21%). The CO_2 drawdown diminishes C_{org} burial, and the second pulse of LIP activity results in the negative Plenus CIE. A subsequent rise in burial, coupled with volcanism cessation, causes "b." These features are not simulated by our stepped scenario (Fig. 3). Atmospheric CO_2 responds directly to changes in LIP activity, whereas the response in C_{org} burial is delayed, modulated by P input and regeneration with longer response time, and leads to a slower response of exogenic $\delta^{13}C$.

CONCLUSION

Our carbon cycle simulations show that two pulses of LIP volcanism, increased terrestrial weathering and P supply, and redox dependent C_{org} and P burial are required to reproduce trends and patterns in global exogenic $\delta^{13}C$, atmospheric pCO_2, and C_{org} burial across OAE2. Our best-fit scenario reproduces the 3‰ onset, $\delta^{13}C$ maxima ("a" and "b"), and the Plenus CIE. The global pCO_2 decrease that occurred near "a" is caused by high C_{org} burial and a pause in LIP volcanism. Subsequent burial reduction and elevated LIP activity result in the Plenus CIE and an increase in pCO_2. The second pCO_2 and C_{org} burial maxima are only present in simulations with a second pulse of volcanism. Our scenario of variable volcanism and C_{org} burial quantitatively explains the key features of the OAE2 carbon cycle and climate dynamics and the relative timing between maximum $\delta^{13}C$, the Plenus CIE, and high pCO_2. We propose that future work should attempt to directly link osmium records to outgassing scenarios and perform carbon cycle perturbation studies that incorporate C/T paleogeography.

ACKNOWLEDGMENTS

This research was funded by The Netherlands Earth System Science Center (NESSC), which is financially supported by the Dutch Ministry of Education, Culture and Science; a NESSC Travel Grant; and the European Research Council (Starting Grant 278364 to C. Slomp, and Consolidator Grant 771497 to A. Sluijs). We thank R. Zeebe and N. Komar, University of Hawai'i, for the LOSCAR-P code and advice. H. Pälike was supported through the Cluster of Excellence "The Ocean Floor–Earth's Uncharted Interface" (research unit recorder), DFG 390741603. We thank M. Jones, I. Jarvis, and J. Owens for their helpful reviews and comments.

REFERENCES CITED

Barclay, R.S., McElwain, J.C., and Sageman, B.B., 2010, Carbon sequestration activated by a volcanic CO_2 pulse during Ocean Anoxic Event 2: Nature Geoscience, v. 3, p. 205–208, https://doi.org/10.1038/ngeo757.

Bond, D.P., and Wignall, P.B., 2014, Large igneous provinces and mass extinctions: An update, *in* Keller, G., and Kerr, A.C., eds., Volcanism, Impacts, and Mass Extinctions: Causes and Effects: Geological Society of America Special Paper 505, p. 29–55, https://doi.org/10.1130/2014.2505(02).

Clarkson, M.O., Stirling, C.H., Jenkyns, H.C., Dickson, A.J., Porcelli, D., Moy, C.M., Pogge von Strandmann, P.A.E., Cooke, I.R., and Lenton, T.M., 2018, Uranium isotope evidence for two episodes of deoxygenation during Oceanic Anoxic Event 2: Proceedings of the National Academy of Sciences of the United States of America, v. 115, p. 2918–2923, https://doi.org/10.1073/pnas.1715278115.

Du Vivier, A.D.C., Selby, D., Condon, D.J., Takashima, R., and Nishi, H., 2015, Pacific $^{187}Os/^{188}Os$ isotope chemistry and U-Pb geochronology: Synchroneity of global Os isotope change across OAE 2: Earth and Planetary Science Letters, v. 428, p. 204–216, https://doi.org/10.1016/j.epsl.2015.07.020.

Forster, A., Schouten, S., Moriya, K., Wilson, P.A., and Sinninghe Damsté, J.S., 2007, Tropical warming and intermittent cooling during the Cenomanian/Turonian Oceanic Anoxic Event 2: Sea surface temperature records from the equatorial Atlantic: Paleoceanography, v. 22, PA1219, https://doi.org/10.1029/2006PA001349.

Gale, A.S., Kennedy, W.J., Voigt, S., and Walaszczyk, I., 2005, Stratigraphy of the Upper Cenomanian–Lower Turonian Chalk succession at Eastbourne, Sussex, UK: Ammonites, inoceramid bivalves and stable carbon isotopes: Cretaceous Research, v. 26, p. 460–487, https://doi.org/10.1016/j.cretres.2005.01.006.

Gangl, S.K., Moy, C.M., Stirling, C.H., Jenkyns, H.C., Crampton, J.S., Clarkson, M.O., Ohneiser, C., and Porcelli, D., 2019, High-resolution records of Oceanic Anoxic Event 2: Insights into the timing, duration and extent of environmental perturbations from the palaeo-South Pacific Ocean: Earth and Planetary Science Letters, v. 518, p. 172–182, https://doi.org/10.1016/j.epsl.2019.04.028.

Jarvis, I., Lignum, J.S., Gröcke, D.R., Jenkyns, H.C., and Pearce, M.A., 2011, Black shale deposition, atmospheric CO_2 drawdown, and cooling during the Cenomanian-Turonian Oceanic Anoxic Event: Paleoceanography, v. 26, PA3201, https://doi.org/10.1029/2010PA002081.

Jenkyns, H.C., 2010, Geochemistry of oceanic anoxic events: Geochemistry Geophysics Geosystems, v. 11, Q03004, https://doi.org/10.1029/2009GC002788.

Jones, M.M., Sageman, B.B., Selby, D., Jicha, B.R., Singer, B.S., and Titus, A.L., 2020, Regional chronostratigraphic synthesis of the Cenomanian-Turonian Oceanic Anoxic Event 2 (OAE2) interval, Western Interior Basin (USA): New Re-Os chemostratigraphy and $^{40}Ar/^{39}Ar$ geochronology: Geological Society of America Bulletin, v. 133, p. 1090–1104, https://doi.org/10.1130/B35594.1.

Jones, M.T., Jerram, D.A., Svensen, H.H., and Grove, C., 2016, The effects of large igneous provinces on the global carbon and sulphur cycles: Palaeogeography, Palaeoclimatology, Palaeoecology, v. 441, p. 4–21, https://doi.org/10.1016/j.palaeo.2015.06.042.

Joo, Y.J., Sageman, B.B., and Hurtgen, M.T., 2020, Data-model comparison reveals key

environmental changes leading to Cenomanian-Turonian Oceanic Anoxic Event 2: Earth-Science Reviews, v. 203, 103123, https://doi.org/10.1016/j.earscirev.2020.103123.

Kalanat, B., Gharaie, M.H.M., Vahidinia, M., and Matsumoto, R., 2018, Short-term eustatic sea-level changes during the Cenomanian–Turonian Supergreenhouse interval in the Kopet-Dagh Basin, NE Tethyan realm: Journal of Iberian Geology, v. 44, p. 177–191, https://doi.org/10.1007/s41513-018-0060-8.

Kerr, A.C., 1998, Oceanic plateau formation: A cause of mass extinction and black shale deposition around the Cenomanian–Turonian boundary?: Journal of the Geological Society, v. 155, p. 619–626, https://doi.org/10.1144/gsjgs.155.4.0619.

Kolonic, S., et al., 2005, Black shale deposition on the northwest African Shelf during the Cenomanian/Turonian oceanic anoxic event: Climate coupling and global organic carbon burial: Paleoceanography, v. 20, https://doi.org/10.1029/2003PA000950.

Komar, N., and Zeebe, R.E., 2017, Redox-controlled carbon and phosphorus burial: A mechanism for enhanced organic carbon sequestration during the PETM: Earth and Planetary Science Letters, v. 479, p. 71–82, https://doi.org/10.1016/j.epsl.2017.09.011.

Kuhnt, W., Holbourn, A.E., Beil, S., Aquit, M., Krawczyk, T., Flögel, S., Chellai, E.H., and Jabour, H., 2017, Unraveling the onset of Cretaceous Oceanic Anoxic Event 2 in an extended sediment archive from the Tarfaya-Laayoune Basin, Morocco: Paleoceanography, v. 32, p. 923–946, https://doi.org/10.1002/2017PA003146.

Kump, L.R., and Arthur, M.A., 1999, Interpreting carbon-isotope excursions: Carbonates and organic matter: Chemical Geology, v. 161, p. 181–198, https://doi.org/10.1016/S0009-2541(99)00086-8.

Kuroda, J., Ogawa, N.O., Tanimizu, M., Coffin, M.F., Tokuyama, H., Kitazato, H., and Ohkouchi, N., 2007, Contemporaneous massive subaerial volcanism and late Cretaceous Oceanic Anoxic Event 2: Earth and Planetary Science Letters, v. 256, p. 211–223, https://doi.org/10.1016/j.epsl.2007.01.027.

Kuypers, M.M.M., Pancost, R.D., Nijenhuis, I.A., and Sinninghe Damsté, J.S., 2002, Enhanced productivity led to increased organic carbon burial in the euxinic North Atlantic basin during the late Cenomanian oceanic anoxic event: Paleoceanography and Paleoclimatology, v. 17, p. 3-1–3-13, https://doi.org/10.1029/2000PA000569.

Li, Y.X., Montañez, I.P., Liu, Z., and Ma, L., 2017, Astronomical constraints on global carbon-cycle perturbation during Oceanic Anoxic Event 2 (OAE2): Earth and Planetary Science Letters, v. 462, p. 35–46, https://doi.org/10.1016/j.epsl.2017.01.007.

Nederbragt, A.J., Thurow, J., Vonhof, H., and Brumsack, H.J., 2004, Modelling oceanic carbon and phosphorus fluxes: Implications for the cause of the late Cenomanian Oceanic Anoxic Event (OAE2): Journal of the Geological Society, v. 161, p. 721–728, https://doi.org/10.1144/0016-764903-075.

O'Connor, L.K., Jenkyns, H.C., Robinson, S.A., Remmelzwaal, S.R., Batenburg, S.J., Parkinson, I.J., and Gale, A.S., 2020, A Re-evaluation of the Plenus Cold Event, and the links between CO_2, temperature, and seawater chemistry during OAE 2: Paleoceanography and Paleoclimatology, v. 35, e2019PA003631.

Owens, J.D., Lyons, T.W., and Lowery, C.M., 2018, Quantifying the missing sink for global organic carbon burial during a Cretaceous oceanic anoxic event: Earth and Planetary Science Letters, v. 499, p. 83–94, https://doi.org/10.1016/j.epsl.2018.07.021.

Reichow, M.K., et al., 2009, The timing and extent of the eruption of the Siberian Traps large igneous province: Implications for the end-Permian environmental crisis: Earth and Planetary Science Letters, v. 277, p. 9–20, https://doi.org/10.1016/j.epsl.2008.09.030.

Self, S., Thordarson, T., and Widdowson, M., 2005, Gas fluxes from flood basalt eruptions: Elements, v. 1, p. 283–287, https://doi.org/10.2113/gselements.1.5.283.

Sinninghe Damsté, J.S., Kuypers, M.M., Pancost, R.D., and Schouten, S., 2008, The carbon isotopic response of algae, (cyano)bacteria, archaea and higher plants to the late Cenomanian perturbation of the global carbon cycle: Insights from biomarkers in black shales from the Cape Verde Basin (DSDP Site 367): Organic Geochemistry, v. 39, p. 1703–1718, https://doi.org/10.1016/j.orggeochem.2008.01.012.

Sinninghe Damsté, J.S., van Bentum, E.C., Reichart, G.J., Pross, J., and Schouten, S., 2010, A CO_2 decrease-driven cooling and increased latitudinal temperature gradient during the mid-Cretaceous Oceanic Anoxic Event 2: Earth and Planetary Science Letters, v. 293, p. 97–103, https://doi.org/10.1016/j.epsl.2010.02.027.

Sullivan, D.L., Brandon, A.D., Eldrett, J., Bergman, S.C., Wright, S., and Minisini, D., 2020, High resolution osmium data record three distinct pulses of magmatic activity during Cretaceous Oceanic Anoxic Event 2 (OAE-2): Geochimica et Cosmochimica Acta, v. 285, p. 257–273, https://doi.org/10.1016/j.gca.2020.04.002.

Tsikos, H., et al., 2004, Carbon-isotope stratigraphy recorded by the Cenomanian–Turonian Oceanic Anoxic Event: Correlation and implications based on three key localities: Journal of the Geological Society, v. 161, p. 711–719, https://doi.org/10.1144/0016-764903-077.

Turgeon, S.C., and Creaser, R.A., 2008, Cretaceous oceanic anoxic event 2 triggered by a massive magmatic episode: Nature, v. 454, p. 323–326, https://doi.org/10.1038/nature07076.

Voigt, S., Aurag, A., Leis, F., and Kaplan, U., 2007, Late Cenomanian to Middle Turonian high-resolution carbon isotope stratigraphy: New data from the Münsterland Cretaceous Basin, Germany: Earth and Planetary Science Letters, v. 253, p. 196–210, https://doi.org/10.1016/j.epsl.2006.10.026.

Voigt, S., Erbacher, J., Mutterlose, J., Weiss, W., Westerhold, T., Wiese, F., Wilmsen, M., and Wonik, T., 2008, The Cenomanian-Turonian of the Wunstorf section (North Germany): Global stratigraphic reference section and new orbital time scale for Oceanic Anoxic Event 2: Newsletters on Stratigraphy, v. 43, p. 65, https://doi.org/10.1127/0078-0421/2008/0043-0065.

Zeebe, R.E., 2012, LOSCAR: Long-term ocean-atmosphere-sediment carbon cycle reservoir model v2.0.4: Geoscientific Model Development, v. 5, p. 149–166, https://doi.org/10.5194/gmd-5-149-2012.

Zeebe, R.E., and Tyrrell, T., 2019, History of carbonate ion concentration over the last 100 million years II: Revised calculations and new data: Geochimica et Cosmochimica Acta, v. 257, p. 373–392, https://doi.org/10.1016/j.gca.2019.02.041.

Printed in USA